Seismic response analyses of piled raft with grid-form DMWs using 3D nonlinear FE model under large earthquake loads

Analyse de la réponse sismique de radiers sur pilotis à DMWs en réseau, utilisant un modèle FE en trois dimensions non-linéaire soumis aux charges d'un gros séisme.

Yoshimasa Shigeno, Kiyoshi Yamashita, Junji Hamada
Takenaka Research & Development Institute, Takenaka Corporation, Japan, shigeno.yoshimasa@takenaka.co.jp

ABSTRACT: The aim of this study is to evaluate seismic performance of a piled raft foundation with grid-form cement deep mixing walls (DMWs) subjected to large earthquake loads. In a previous study, seismic simulation analyses of the piled raft using 3D nonlinear FE soil model against medium earthquake loads were carried out successfully, and the earthquake loads were based on the observation site records of the 2011 off the Pacific Coast of Tohoku Earthquake. Large earthquake load is caused by inputting the ground motion that is defined by 500 years recurrence interval being used for a building design in Japan. Three cases are examined. Two cases are with the different strength DMWs, and one case is without DMWs. As a result, partial tensile failure occurred in DMWs, however, the bending moment of the piles is markedly smaller compared to the case without DMWs. And the sectional force of the piles is reduced to an acceptable level. This indicates that the grid-form DMWs are quite effective in reducing the sectional force of piles under large earthquake load, even if the induced stress in the DMWs partially reaches its tensile strength.

RÉSUMÉ : Le but de cette étude est l'évaluation du comportement sismique de fondations à radiers sur pilotis équipées de murs de ciment composite profonds en réseau (DMWs), mis à l'epreuve des charges d'un gros séisme. Dans une étude précédente, nous avions réalisé avec succès des analyses de simulation sismique du radier sur pilotis en utilisant un modèle FE non-linéaire 3D impliquant des charges sismiques. Ces charges sismiques étaient basées sur des données enregistrées sur site lors du Grand Séisme du Tohoku en 2011. De grandes charges sismiques sont obtenues en tenant compte des mouvements du sol définis par l'intervalle de récurrence à 500 ans, une valeur utilisée dans la conception des bâtiments au Japon. Nous avons examiné trois modèles: dans deux cas, on mit en œuvre des DMWs de forces différentes et dans un cas, sans intervention de DMWs; cependant le moment de torsion des pilotis était remarquablement plus petit que dans le cas sans DMWs. La force sur la section des pilotis en est réduite à un niveau acceptable. Ceci montre que les DMWs en réseau sont très efficaces pour réduire les forces exercées sur les pilotis sous les charges d'un gros séisme, même si le stress induit dans les DMWs atteint partiellement ses forces de tension.

KEYWORDS: piled raft foundation, grid-form DMWs, large earthquake, soil and structure interaction analysis, FEM.

1 INTRODUCTION

The aim of this study is to evaluate seismic performance of a piled raft foundation with grid-form cement deep mixing walls (DMWs) subjected to large earthquake loads. Seismic simulation analyses of the piled raft using 3D nonlinear FE soil model against medium earthquake loads were carried out successfully in the previous study (Shigeno et al, 2016). In this paper, to evaluate the induced internal stresses in the DMWs against their capacity, a nonlinear-elastic model with tensile and shear criteria is applied for the stabilized soil, and the effect of partial failure of the DMWs caused by the strong motion on the sectional force of the piles is mainly discussed.

2 BUILDING AND GROUND CONDITIONS

Figure 1 shows a schematic view of a 12-story residential building with soil profile. The building, a reinforced concrete structure with a seismic base isolation system, is located in Tokyo. The subsoil consists of an alluvial stratum to a depth of 44 m underlain very dense sand-and gravel. The soil profile down to a depth of 7 m is fill and loose silty sand. Between the depths of 7 m and 44 m, the profile is very soft to medium silty clay. The building is supported by a piled raft foundation combined with grid-form DMWs which are employed to prevent liquefaction of the silty sand below the raft as well as to improve the bearing capacity of the raft foundation. At the time of the 2011 off the Pacific Coast of Tohoku Earthquake, the seismic response of the soil-foundation system was successfully recorded (Yamashita et al., 2012).

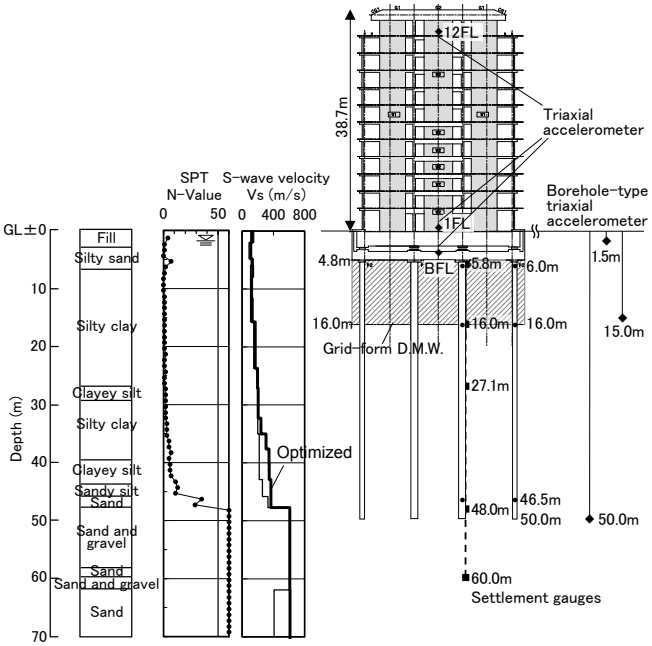

Figure 1. Schematic view of building and foundation with soil profile.

3 NUMERICAL ANALYSES

3 .1 *Finite element mesh*

Figure 2 shows the finite element (FE) mesh. The number of elements is 213,622 and the number of degrees-of-freedom is

656,543. Figure 3 shows the top view of the FE mesh beneath the raft. To consider the shape and volume of the piles, cavities in the shape of the piles are made in the FE model. The nodes of the piles and the adjacent ground nodes at the same depth are bound by rigid bar elements. The base isolation layer is modeled by tri-linear spring elements. The lateral boundaries are periodic boundaries. They are positioned at 60 m outside of the building to minimize the boundary effect. The bottom is a viscous boundary. The engineering bedrock is set at a depth of 75m from the ground surface. The building is modeled by elastic bars and shells and the piles are also modeled by elastic bars. Table 1 shows the material properties of the piles.

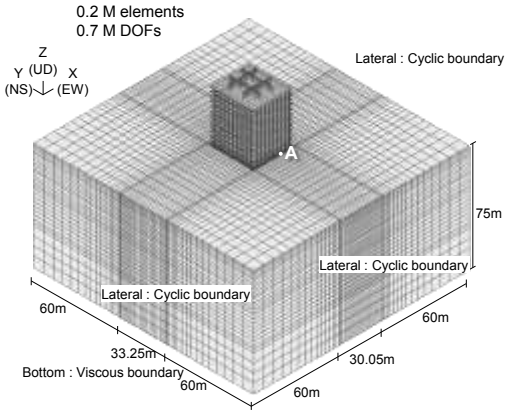

Figure 2. Finite element mesh of soil-structure model.

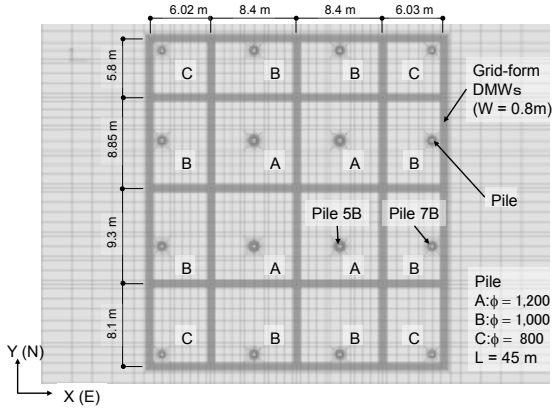

Figure 3. Plan view of FE mesh beneath the raft.

Table 1. Material characteristics of piles.

Pile diameter	(mm)	800	1000	1200
Young's modulus	(MN/m^2)	40000	40000	40000
Damping	(%)	2	2	2
Ae of SC pile	(m^2)	0.3268	0.4649	0.6714
Ie of SC pile	(m^4)	0.02199	0.04899	0.10316
Ae of PHC pile	(m^2)	0.2441	0.3633	0.5054
Ie of PHC pile	(m^4)	0.01455	0.03437	0.06958

Ae : Equivalent cross-sectional area, Ie : Equivalent moment of inertia of area

3 .2 *Input motion*

A large earthquake has been chosen from level 2 waves that are officially notified in Japanese design code. Level 2 waves are used for the performance design of building. The waves are defined according to the response spectrum and generated using phase data. In this paper, the Hachinohe phase data that was recorded at Tokachi - Oki Earthquake (1968) at Hachinohe Bay is used as a subduction zone earthquake. Figure 4 shows the input acceleration in the NS direction at the bedrock (the wave is 2E). The time interval is 0.005 s and the analysis time is 120 s. Figure 5 shows the acceleration response spectrum of the input wave. The analysis code is an in-house program called MuDIAN. This code is parallelized by the hybrid parallel method and is able to calculate a large degrees-of-freedom model with high speed.

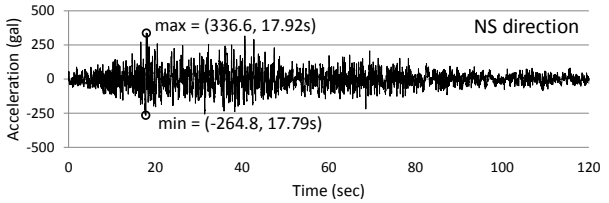

Figure 4. Input acceleration of level 2 Hachinohe phase at depth of 75m (2E).

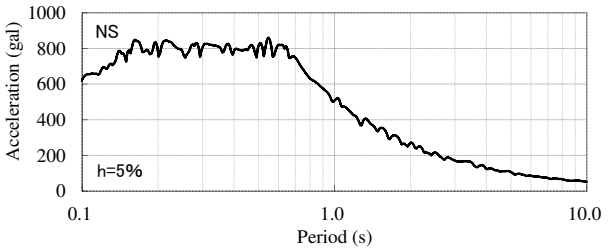

Figure 5 Acceleration response spectrum of input motion.

3 .3 *Constitutive model and properties of soil*

The Yoshida model for multi-dimension (Tsujino et. al., 1994) is used as the constitutive model for the soil. The Yoshida model is a multi-surface model and is characterized using G-γ and h-γ characteristics directly as input data, and the model uses a non-linear elastic stress–strain relation.

The shear wave velocity profile of the ground for the analysis is shown in Fig. 1 together with that derived from P-S logging. The shear wave velocity profile was obtained by optimizing the error of the transfer function. The P-S logging results were used as the initial Vs. And small earthquakes that occurred before the 2011 off the Pacific coast of Tohoku Earthquake were used as target data (Hamada et al., 2014).

Figure 6 shows the G-γ and h-γ relations of each soil layer at this site. The τ_{max} of each layer is assumed so that the modeled τ-γ curve calculated from G-γ curve fits the τ-γ curve of the test data within 4% shear strain. Initial damping other than the damping induced by the constitutive model is assumed 1%, and is given by Rayleigh damping.

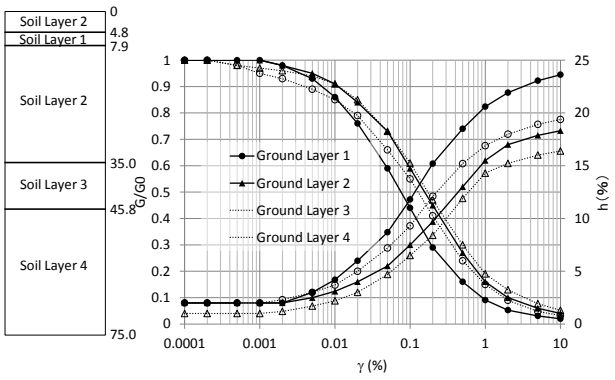

Figure 6. Strain dependence characteristics of soil.

3 .4 *Constitutive model of stabilized soil*

The failure of the DMWs is caused by tensile or shear. Both the tensile and shear criteria have to be used to evaluate the correct strength. Maximum principal stress σ_1 which means the maximum tensile stress (note that tension is plus) is expressed by the second deviate stress invariants J'_2, mean stress σ_m and Lode angle θ. The tensile strength σ_t is expressed as follows.

$$\sigma_t = \sigma_1 = \frac{2(J'_2)^{\frac{1}{2}}}{\sqrt{3}} \sin\left(\theta + \frac{2\pi}{3}\right) + \sigma_m \qquad (1)$$

And the Mohr–Coulomb criterion for the shear failure is expressed by stress invariants, friction angle ϕ and cohesion c.

$$\sigma_m \sin\phi + (J'_2)^{\frac{1}{2}}\left(\cos\theta - \frac{1}{\sqrt{3}}\sin\theta\sin\phi\right) = c\cos\phi \qquad (2)$$

The strength is taken lower value between the two criteria.

The Hayashi–Hibino model (Motojima et al., 1978) is used as a two criteria model in this study. The Hayashi–Hibino model is a nonlinear elastic model. Elastic modulus reduces to the user specified value at the failure. This model is also able to express nonlinearity before failure using the proximity ratio to the criteria R. The elastic moduli are reduced according to R in the following equations using the nonlinear parameter a.

$$E = R^{1/a} E_0, \qquad 0.45 - \nu = R^{1/2a}(0.45 - \nu_0) \qquad (3)$$

3 .5 *Properties of stabilized soil*

Two sets of properties are set based on the compressive strength as shown in Table 2. In case 1, the design standard compressive strength F_c is used, and in case2, the compressive strength of in-situ sampling core q_{uf} is used. The value of q_{uf} is 3.8 MPa that is the average value of 36 core samples aged 28 days (Yamashita et al., 2015). The value of F_c is 2.6 MPa that is calculated referred to BCJ (2002) following the equation (4)

$$F_c = (1 - 1.3\, V_{q_{uf}})\, q_{uf} \qquad (4)$$

where $V_{q_{uf}}$ is the variation of q_{uf} (= 0.25). The tensile strength and the cohesion are 0.2 and 0.3 times the compressive strength respectively quoted from Namikawa (2007). The friction angle and the Poisson's ratio are assumed to be 30 degrees and 0.26 referred to BCJ (2002).

The nonlinear parameter a is obtained by simulating simple shear test to fit the G-γ curve reported by Kuroda et al. (2001) as shown in Fig. 7. Damping of the stabilized soil is needed because the model is nonlinear elastic. The damping ratio is assumed to be 5% referred to Kuroda et al. (2001). The initial shear modulus (G_0 = 500 MPa) was determined based on the analysis using the observation records (Shigeno et al., 2016).

As for the initial stress in the DMWs, isotropic stress of 170 kPa is given by considering the measured vertical pressure between the raft and the DMWs of 300 kPa (Yamashita et al, 2015) and the horizontal stress calculated using the coefficient of earth pressure at rest.

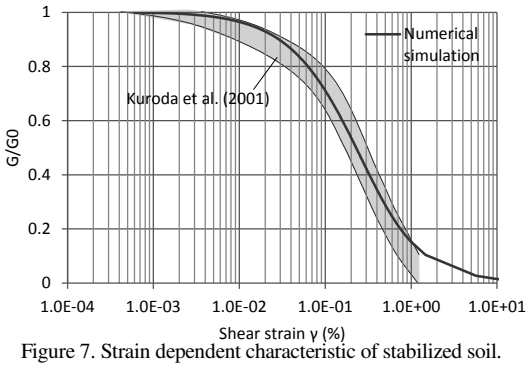

Figure 7. Strain dependent characteristic of stabilized soil.

4 RESULTS OF SEISMIC RESPONSE ANALYSES

The case without the grid-form DMWs is also conducted as case3 to clarify the effect of the DMWs. Figure 8 shows the profiles of the peak acceleration of the center of the structure and the ground at a point A (Fig. 2). Results of case1 and case2 are almost the same, then only case 1 and case 3 are shown. The response of the soil column model is also shown as the far field, and the PGA is 2.95 m/s^2. The peak acceleration of the raft, at a depth of 4.8 m, is 2.65-2.78m/s^2. In contrast, the peak acceleration on the first floor is 1.08-1.31 m/s^2, which is reduced to 41-47% of the ground due to the base isolation system. Figure 9 shows the profiles of the peak displacement relative to the depth of 50 m. The peak ground displacements occur asymmetrically due to nonlinearity of the soil, and are fairly larger in the southern direction. Moreover, the ground displacements are different due to existence of the DMWs. The peak displacement at the top surface of the DMWs (at the depth of 4.8 m) is 0.11 m in case 1, which is considerably smaller than that of in case 3 (0.16 m). The ground deformation beneath the raft is significantly decreased by the DMWs.

Figure 10 shows the profiles of the peak bending moment in Piles 5B and 7B. The peak bending moments near the pile head show asymmetry in consistent with the ground deformation. Furthermore, the peak bending moments near the pile head in cases 1 are markedly smaller than those in cases 3. This is because a considerable amount of the horizontal force is carried by the DMWs while the ground deformation beneath the raft is decreased by the DMWs. Here, the horizontal force means the sum of the inertial force from the superstructure and passive force acting on the sides of the buried raft.

Figure 11 illustrates the extent of tensile failure in the grid-form DMWs in case 1. Elements are colored according to the number of Gauss points that tensile failure occur. Number of Gauss points is eight in each element. The tensile failure occurred in limited elements, and they are seen mostly in the longitudinal walls. This suggests that the lateral external force acting on the top surface of the DMWs is carried mainly by the longitudinal walls. In case 2, fewer elements fail than case 1. Moreover, shear failure is not almost seen in both cases. Considering the similarity with the case 2, the limited failure zones in case 1 do not affect much on the response.

Figure 12 shows the relationship between the axial force and the bending moment of Piles 5B and 7B, together with the design interaction curves of the steel pipe-concrete composite

Table 2. Properties of stabilized soil and parameters of Hayashi–Hibino model.

	Density ρ (t/m^3)	Compressive strength q (MPa)	Tensile strength σ_t (MPa)	Cohesion c (MPa)	Friction angle φ (degree)	Shear modulus G_0 (MPa)	ν	Damping h (%)	Nonlinear Parameter a	G/G_0 after failure
case 1	2.0	2.60	0.52	0.78	30	500	0.26	5.0	1.0	1.0e-5
case 2	2.0	3.80	0.76	1.14	30	500	0.26	5.0	1.5	1.0e-5

(SC) pile which is used in the top portion of 12 m. Here, the axial force means the sum of the statically measured pile head load and the peak dynamic incremental forces in the analysis, and the bending moment means the maximum value along the SC pile. The numerical results indicate that the maximum bending moments in cases 1 are below the allowable criterion (unit stress at the edge of concrete is in elastic condition). In contrast, the maximum bending moments in case 3 are clearly beyond the allowable criterion. Hence, the grid-form DMWs are quite effective in reducing pile bending moments to an allowable level, even if the induced stress in the DMWs reaches partially the tensile strength under the large earthquake load.

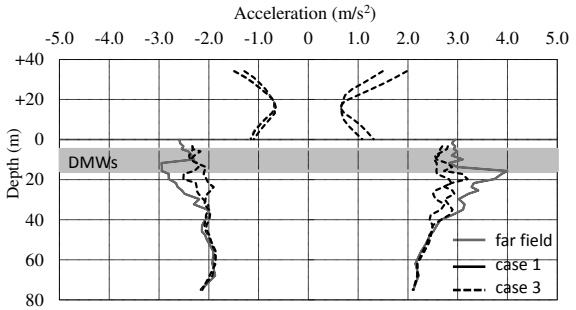

Figure 8. Profiles of peak acceleration of structure and ground.

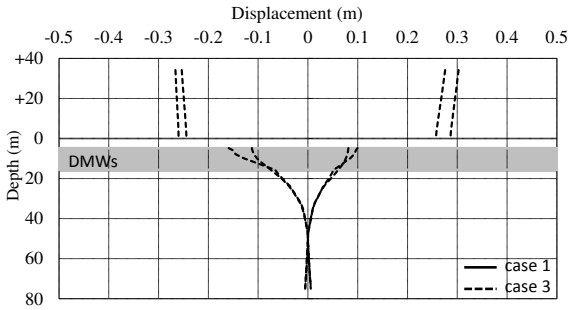

Figure 9. Profiles of peak relative displacement of structure and ground.

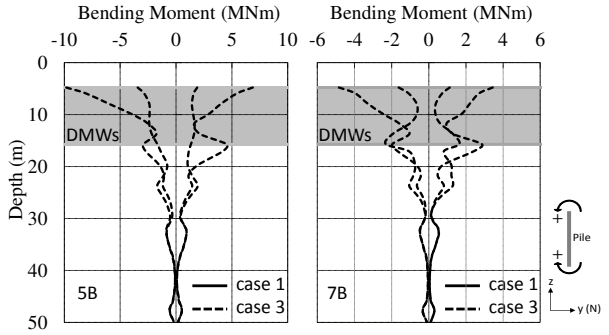

Figure 10 Profiles of maximum bending moment of piles 5B and 7B.

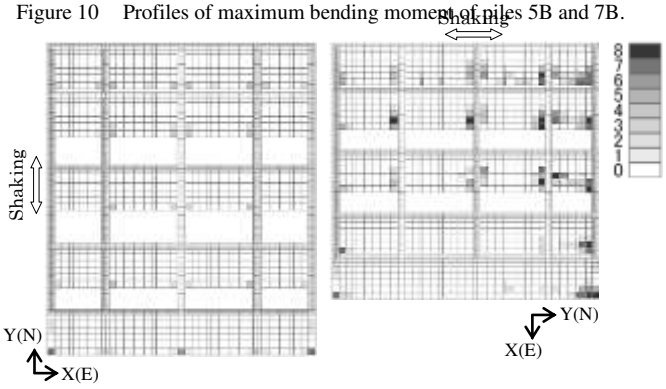

Figure 11. Tensile failure Gauss points in grid-form DMWs.

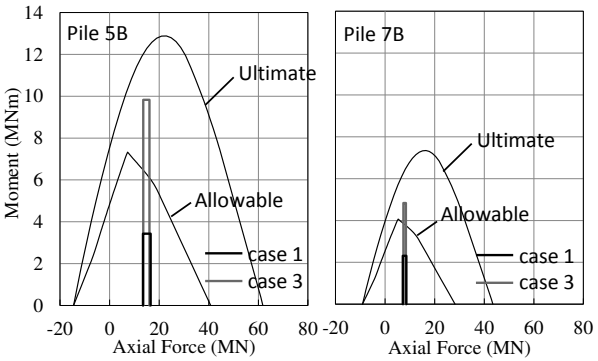

Figure 12. NM-relationship of SC piles, and calculated values.

Namikawa et al (2007) have pointed out that the grid-form DMWs can be designed more rationally by the performance-based design method in which a partial failure of the DMWs is accepted. The numerical results suggest that the present nonlinear 3D FE model can provide adequate solutions for the performance-based seismic design of piled rafts with the grid-form DMWs.

5 CONCLUSION

Seismic response analyses of a piled raft foundation with grid-form DMWs using 3D nonlinear FE model under large earthquake loads were carried out based on the previous successful simulation analyses against medium earthquake loads. Consequently, it was found that the grid-form DMWs are quite effective in reducing sectional force of the piles to an acceptable level under large earthquake loads, even if partial tensile and/or shear failure occur in the stabilized soil.

6 REFERENCES

Shigeno,Y., Hamada, J., Nakamura, H. and Yamashita, K. 2016. Seismic Performance of Piled Raft Foundation with Grid-Form DMWs under Large Earthquake Load, *Takenaka Technical Research Report*, No.72 (in printing)

Yamashita, K., Hamada, J., Onimaru, S. and Higashino, M. 2012. Seismic behavior of piled raft with ground improvement supporting a base-isolated building on soft ground in Tokyo, *Soils & Foundations*, Special Issue on Geotechnical Aspects of the 2011 off the Pacific Coast of Tohoku Earthquake, Vol.52(5), 1000-1015.

Hamada, J., Shigeno, Y., Onimaru, S., Tanikawa, T., Nakamura, N. and Yamashita, K. 2014. Numerical analysis on seismic response of piled raft foundation with ground improvement based on seismic observation records, *Proc. of the 14th IACMAG*.

Tsujino, S., Yoshida, N. and Yasuda, S. 1994. A simplified practical stress-strain model in multi-dimensional analysis, *Proc., International Symposium on Pre-failure Deformation Characteristics of geomaterials*, Sapporo, pp. 463-468.

Motojima, M., Hibino S. and Hayashi, M. 1978. Development of computer program for stability analysis of excavation, *Central Research Institute of Electric Power Industry Report* No 377012 (in Japanese).

Yamashita, K., Tanikawa, T., Shigeno, Y. and Hamada, J., 2015. Vertical load sharing of piled raft with grid-form deep mixing walls, *Proc. of Conference on Deep Mixing 2015*, 437–446.Building Center of Japan, 2002. *Specification for design and quality control of cement treated soil* (in Japanese).

Kuroda, T., Tanaka, H., Tomii, Y., Suzuki, Y., 2001. Evaluation of characteristics of improved soil by the deep mixing method of soil stabilization, Study on dynamic deformation characteristics of improved soil (Part 3), *Summaries of technical papers of annual meeting AIJ*, B-1, 699-700 (in Japanese).

Namikawa, T., Koseki, J. and Suzuki, Y. 2007. Finite element analysis of lattice-shaped ground improvement by cement-mixing for liquefaction mitigation, *Soils & Foundations*, Vol.47(3), 559-576.